# Different variants of R13 moment equations applied to the shock-wave structure

M. Yu. Timokhin, H. Struchtrup, A. A. Kokhanchik, and Ye. A. Bondar

Citation: Physics of Fluids **29**, 037105 (2017); doi: 10.1063/1.4977978
View online: http://dx.doi.org/10.1063/1.4977978
View Table of Contents: http://aip.scitation.org/toc/phf/29/3
Published by the American Institute of Physics

# Different variants of R13 moment equations applied to the shock-wave structure

M. Yu. Timokhin,[1,2,a)] H. Struchtrup,[3,b)] A. A. Kokhanchik,[4,5,c)] and Ye. A. Bondar[4,5,6,d)]
[1]*Moscow State University, 119991 Moscow, Russia*
[2]*Moscow Aviation Institute, 125993 Moscow, Russia*
[3]*Department of Mechanical Engineering, University of Victoria, Victoria, British Columbia V8W 2Y2, Canada*
[4]*Khristianovich Institute of Theoretical and Applied Mechanics SB RAS (ITAM), 630090 Novosibirsk, Russia*
[5]*Novosibirsk State University, 630090 Novosibirsk, Russia*
[6]*Saint Petersburg State University, 199034 St. Petersburg, Russia*

(Received 23 December 2016; accepted 21 February 2017; published online 14 March 2017; corrected 30 March 2017)

Various versions of the regularized 13-moment system (R13) are applied to the problem of the shock wave structure in a monatomic Maxwell gas for Mach numbers up to M = 10. Numerical solutions are compared to direct simulation Monte Carlo results computed by the SMILE++ software system, in order to identify applicability and limitations of the variants. Over time, several versions of the R13 equations were presented, which differ in non-linear contributions for high-order moments but agree in asymptotic expansion to the third order in the Knudsen number. All variants describe typical subsonic microflows well, for which the non-linear contributions only play a minor role. The challenge of the present study is to determine the real boundaries of applicability of each variant of the moment equations as applied to non-equilibrium supersonic flows, depending on the Mach number and local Knudsen number. *Published by AIP Publishing.* [http://dx.doi.org/10.1063/1.4977978]

## I. INTRODUCTION

Macroscopic equations for rarefied flows can be derived as approximations to the Boltzmann equation, with the goal to have faster numerical calculations, or even exact solutions, while allowing for some inaccuracy due to the approximation. The Navier-Stokes and Fourier (NSF) equations[1,2] of classical hydrodynamics serve this purpose well only for sufficiently small Knudsen numbers Kn.[2–4] The Knudsen number is defined as the ratio of the average mean free path of a particle to the typical length scale of the process, and the NSF equations are limited to processes with, approximately, $\mathrm{Kn} < 0.05$.[3] For processes in the transition regime, where, approximately, $0.01 < \mathrm{Kn} < 10$, extensions of the hydrodynamic equations are based either on the Chapman-Enskog method[2–4] or on Grad's moment method.[3–5]

By asymptotic expansion of the Boltzmann equation, the Chapman-Enskog method derives macroscopic expressions for stresses and heat flux in terms of higher order gradients of temperature and gas velocity. The resulting Burnett and super-Burnett equations[6,7] are unstable for time dependent processes[8] and show inconsistencies in steady state processes,[9] hence are not often used in their original form. Modifications exist, which correct some of these problems, see, e.g., Refs. 10 and 11.

Grad's moment method extends the set of hydrodynamic variables, by including stress, heat flux, and, possibly, higher moments of the velocity distribution function.[3,5] Transport equations for the additional variables are derived by taking moments of the Boltzmann equation. Since the transport equations contain some higher moments, which are not in the list of variables, the method requires an approximation of the velocity distribution function to obtain a closed set of macroscopic transport equations. For this, the Grad method uses an expansion around equilibrium, where the expansion coefficients are related to the variables.[5] The resulting sets of moment equations are linearly stable, but due to their hyperbolic nature[11] they exhibit sharp shocks for supersonic flows, which are an artefact of the theory.

The regularization of Grad-type moment equations aims at improving the Grad closure by accounting for the influence of higher moments.[12] To this end, ideas of the Chapman-Enskog method are used to reduce a larger set of Grad-type moment equations to a more compact set that is the accurate reduction of the larger system to a given order in the Knudsen number. The regularized 13 moment (R13) equations arise as the appropriate equations at third order in Kn (super-Burnett level) and correct Grad's celebrated 13 moment system by adding some higher order terms that are remnants of the transport equations for higher moments.[5,12] The corrections lead to second order derivatives in the R13 equations and change their mathematical character from (mostly) hyperbolic to (mostly) parabolic.

Indeed, in the context of this approach, the parabolic NSF equations appear as the regularization of the hyperbolic Euler equations, where Euler is of zeroth order in Kn and NSF is of first order. The relation between Grad's 13 moment equations and the R13 equations is similar, with the equations at second and third orders in Kn. However, the mathematical structure of the equations is not as clear, e.g., far from equilibrium Grad 13 will lose hyperbolicity,[13,14] and R13

a)timokhin@physics.msu.ru
b)struchtr@uvic.ca
c)alecsei_k_t2@mail.ru
d)bond@itam.nsc.ru

is of mixed type. And just as the Euler equations predict sharp shock and the NSF equations predict smooth shock structures,[13,14] the R13 equations promise smooth shock structures without the subshocks that appear in solutions of the Grad 13 equations.[3,15]

While one of the early contributions on the R13 equations examined their ability to describe one-dimensional shock structures,[15] the subsequent examination focused mainly on subsonic microflows. An important step towards this was the derivation of reliable boundary conditions for the equations, which were presented in Ref. 16 and then refined in Ref. 17. By solving boundary value problems for microflows, both analytically and numerically, and comparing the results to solutions of the underlying Boltzmann equation, the R13 equations were shown to give a good description of all relevant rarefaction effects, such as jump and slip, transpiration flow, Knudsen layers, thermal stresses and non-Fourier heat flux, and shock structures, see the review papers[18,19] for detailed discussion and references.

Over the years, due to refinement of the derivation of the equations and their boundary conditions, a number of different variants of the R13 equations were suggested, with differences particularly in the non-linear contributions to higher moments. All variants agree in the sense that their Chapman-Enskog expansion[2] to super-Burnett order, i.e., third order in Kn, yields the same result. Moreover, the R13 equations show great success for microflows, for which the non-linear terms play only a minor role, and can often be ignored. However, the full non-linear equations differ between variants, and hence show different behavior for flows in which non-linearities play a marked role. The goal of the present study is to examine the different variants for their ability to describe shock structures in good agreement to solutions of the Boltzmann equation. Results of computations by the Direct Simulation Monte Carlo (DSMC) method[20] are considered in the present paper as the solution of the Boltzmann equation. It was demonstrated in Ref. 21 that for the shock wave problem the DSMC results completely coincide with the direct deterministic solution of the Boltzmann equation in terms of velocity distribution function and fine specific features of the shock structure, such as the temperature overshoot. The results presented here are the extended version of our study.[22]

We note that the shock structure is a difficult test for all hydrodynamic models, such as moment equations or Burnett-type equations. Indeed, hydrodynamic models are derived based on the assumption of sufficiently small Knudsen number (to some power). The shock thickness varies with the Mach number, and the corresponding Knudsen number—mean free path over shock thickness—will violate the expansion criterion for stronger shocks of M > 2. For many problems, fine details of the shock structure might not be important, and a qualitative description of the shock might suffice. The results presented below show that for moderate Mach numbers (M = 2) all R13 variants describe the shock structure with a sufficient quantitative accuracy. For larger Mach numbers (M = 4, M = 8), however, the different variants show more marked deviations, with only few variants leading to shock structures that might be considered as acceptable even when only a quantitative description is required. These variants can be used for flows with larger Mach numbers, without large loss of accuracy.

The remainder of the paper proceeds as follows: The R13 variants are presented in Section II in the chronological order, together with some background on the various reasons for modification. Numerical shock structure solutions for Mach numbers up to M = 8 are presented and discussed in detail in Section III. The paper ends with our conclusions in Sec. IV.

## II. R13 VARIANTS

The regularization of the Grad's original 13-moment system[5] was derived in 2003[12] by a Chapman-Enskog expansion[2] of higher moment equations only, based on the assumption of faster relaxation times for higher moments. Since relaxation times for moments only vary slightly between different moments, this assumption is somewhat artificial. Later derivations of the R13 equations were developed explicitly without this assumption (order of magnitude method). Nevertheless, the resulting equations are meaningful and, since they contain some higher order terms, behave well in the description of shocks, as will be seen below. The tensor form of the regularized 13-moment system (R13) can be written as

$$\frac{\partial \rho}{\partial t} + \frac{\partial \rho v_k}{\partial x_k} = 0, \tag{1}$$

$$\rho \frac{\partial v_i}{\partial t} + \rho v_k \frac{\partial v_i}{\partial x_k} + \frac{\partial p}{\partial x_i} + \frac{\partial \sigma_{ik}}{\partial x_k} = 0, \tag{2}$$

$$\frac{3}{2}\rho \frac{\partial \theta}{\partial t} + \frac{3}{2}\rho v_k \frac{\partial \theta}{\partial x_k} + \frac{\partial q_k}{\partial x_k} + p\frac{\partial v_k}{\partial x_k} + \sigma_{ij}\frac{\partial v_i}{\partial x_j} = 0, \tag{3}$$

$$\frac{\partial \sigma_{ij}}{\partial t} + \frac{\partial \sigma_{ij} v_k}{\partial x_k} + \frac{4}{5}\frac{\partial q_{\langle i}}{\partial x_{j\rangle}} + 2p\frac{\partial v_{\langle i}}{\partial x_{j\rangle}} + 2\sigma_{k\langle i}\frac{\partial v_{j\rangle}}{\partial x_k} + \frac{\partial m_{ijk}}{\partial x_k} = -\frac{\sigma_{ij}}{\tau}, \tag{4}$$

$$\frac{\partial q_i}{\partial t} + \frac{\partial q_i v_k}{\partial x_k} + \frac{5}{2}p\frac{\partial \theta}{\partial x_i} + \frac{5}{2}\sigma_{ik}\frac{\partial \theta}{\partial x_k} + \theta\frac{\partial \sigma_{ik}}{\partial x_k} - \sigma_{ik}\theta\frac{\partial \rho}{\partial x_k} - \frac{\sigma_{ij}}{\rho}\frac{\partial \sigma_{jk}}{\partial x_k} + \frac{7}{5}q_k\frac{\partial v_i}{\partial x_k} + \frac{2}{5}q_k\frac{\partial v_k}{\partial x_i} + \frac{2}{5}q_i\frac{\partial v_k}{\partial x_k} + \frac{1}{2}\frac{\partial R_{ik}}{\partial x_k} + \frac{1}{6}\frac{\partial \Delta}{\partial x_i} + m_{ijk}\frac{\partial v_j}{\partial x_k} = -\frac{2}{3}\frac{q_i}{\tau}, \tag{5}$$

where the mass density $\rho$, velocity $v_i$, temperature in energy units $\theta = \frac{k}{m}T$ ($k$ is the Boltzmann constant and $m$ the particle mass), trace-free viscous stress tensor $\sigma_{ij}$ (with $\sigma_{ii} = 0$), and heat flux $q_i$ ($i = x, y, z$) form 13 primitive variables. The pressure is given by the ideal gas law $p = \rho\theta$, and $\tau = \mu/p$ is the relaxation time, with the viscosity coefficient $\mu$. The angular brackets in the subscripts indicate the trace-free and symmetric part of the tensor.[3] Equations (1)–(3) are the conservation laws for mass, momentum, and energy; Equations (4) and (5) are the moment equations for stress tensor and heat flux vector, respectively. These 13 equations must be closed by constitutive relations for the higher moments $R_{ij}$, $\Delta$, $m_{ijk}$, and these differ based on the method of (regularizing) closure, as discussed next. For Grad's original 13 moment equations,[5] $R_{ij} = \Delta = m_{ijk} = 0$.

The NSF equations of classical hydrodynamics can be obtained from the above by the Chapman-Enskog expansion, which yields the Navier-Stokes and Fourier laws as

$$\sigma_{ij}^{NSF} = -2\mu\frac{\partial v_{\langle i}}{\partial x_{j\rangle}},\ q_i^{NSF} = -\frac{15}{4}\mu\frac{\partial\theta}{\partial x_i}. \tag{6}$$

### A. Original variant (2003)

The original variant of the R13 system obtained by Struchtrup and Torrilhon[12] in 2003 can be written as

$$\Delta = -12\tau\left[\theta\frac{\partial q_k}{\partial x_k} + \frac{5}{2}q_k\frac{\partial\theta}{\partial x_k} - \theta q_k\frac{\partial\ln\rho}{\partial x_k} + \theta\sigma_{ij}\frac{\partial v_i}{\partial x_j} + \underline{\frac{1}{\rho}q_j\frac{\partial\sigma_{jk}}{\partial x_k}}\right], \tag{7}$$

$$R_{ij} = -\frac{24}{5}\tau\left[\theta\frac{\partial q_{\langle i}}{\partial x_{j\rangle}} + q_{\langle i}\frac{\partial\theta}{\partial x_{j\rangle}} - \theta q_{\langle i}\frac{\partial\ln\rho}{\partial x_{j\rangle}} + \frac{5}{7}\theta\left(\sigma_{k\langle i}\frac{\partial v_{j\rangle}}{\partial x_k} + \sigma_{ki}\frac{\partial v_k}{\partial x_j} - \frac{2}{3}\sigma_{ij}\frac{\partial v_k}{\partial x_k}\right) - \underline{\frac{1}{\rho}q_{\langle i}\frac{\partial\sigma_{j\rangle k}}{\partial x_k} - \frac{5}{6}\frac{\sigma_{ij}}{\rho}\frac{\partial q_k}{\partial x_k} - \frac{5}{6}\frac{\sigma_{ij}}{\rho}\sigma_{kl}\frac{\partial v_k}{\partial x_l}}\right], \tag{8}$$

$$m_{ijk} = -2\tau\left[\theta\frac{\partial\sigma_{\langle ij}}{\partial x_{k\rangle}} - \theta\sigma_{\langle ij}\frac{\partial\ln\rho}{\partial x_{k\rangle}} + \frac{4}{5}q_{\langle i}\frac{\partial v_j}{\partial x_{k\rangle}} - \underline{\frac{\partial\sigma_{\langle ij}}{\rho}\frac{\partial\sigma_{k\rangle l}}{\partial x_l}}\right]. \tag{9}$$

Linearization around equilibrium reduces the equations to

$$\Delta = -12\tau\theta\frac{\partial q_l}{\partial x_l},\ R_{ij} = -\frac{24}{5}\tau\theta\frac{\partial q_{\langle i}}{\partial x_{j\rangle}},\ m_{ijk} = -2\tau\theta\frac{\partial\sigma_{\langle ij}}{\partial x_{k\rangle}}. \tag{10}$$

These terms provide the gradient transport mechanism (GTM)[23] for the stress tensor and heat flux. The remaining terms omitted in the linear case form the so-called non-gradient transport mechanism (NGTM).[24] The linear variant (10) and the original nonlinear variant (7)–(9) without underlined terms were studied for shock structures in Refs. 25 and 26; the complete equations including the underlined terms were solved in Ref. 3.

The constitutive relations (7)–(9) can be written in a more compact form by using the equation of state for an ideal gas and the Navier-Stokes and Fourier laws, so that

$$\Delta = 6\frac{\sigma_{kl}\sigma_{kl}^{NSF}}{\rho} + \frac{56}{5}\frac{q_k q_k^{NSF}}{p} - 12\mu\theta\frac{\partial}{\partial x_k}\left(\frac{q_k}{p}\right) + \underline{12\frac{\mu}{p}\frac{q_k}{\rho}\frac{\partial\sigma_{kl}}{\partial x_l}}, \tag{11}$$

$$R_{ij} = \frac{24}{7}\frac{\sigma_{k\langle i}\sigma_{j\rangle k}^{NSF}}{\rho} + \frac{64}{25}\frac{q_{\langle i}q_{j\rangle}^{NSF}}{p} - \frac{24}{5}\mu\theta\frac{\partial}{\partial x_{\langle i}}\left(\frac{q_{j\rangle}}{p}\right) + \underline{\frac{24}{5}\frac{\mu}{p}\frac{q_{\langle i}}{\rho}\frac{\partial\sigma_{j\rangle k}}{\partial x_k} + 4\frac{\mu\theta}{p^2}\sigma_{ij}\frac{\partial q_k}{\partial x_k} + 4\frac{\mu\theta}{p^2}\sigma_{ij}\sigma_{kl}\frac{\partial v_k}{\partial x_l}}, \tag{12}$$

$$m_{ijk} = \frac{8}{15}\frac{\sigma_{\langle ij}q_{k\rangle}^{NSF}}{p} + \frac{4}{5}\frac{q_{\langle i}\sigma_{jk\rangle}^{NSF}}{p} - 2\mu\theta\frac{\partial}{\partial x_{\langle i}}\left(\frac{\partial\sigma_{jk\rangle}}{p}\right) + \underline{2\frac{\mu\theta}{p^2}\sigma_{\langle ij}\frac{\partial\sigma_{k\rangle l}}{\partial x_l}}. \tag{13}$$

The underlined terms of Eqs. (7)–(9) and (11)–(13) turn out to be of 4th order in the Knudsen number;[3] hence they do not contribute to the super-Burnett order. It should be noted that full balance laws for $\Delta$, $R_{ij}$, and $m_{ijk}$ are required to include all terms at 4th order.[3]

### B. Order of magnitude closure (2005)

Struchtrup[3] proposed a new variant of relations for high-order moments, based on a careful examination of the order of magnitude in the Knudsen number of all terms in the equations. Here, and in all variants discussed further, the fourth-order terms with respect to the Knudsen number are ignored. However, as compared to Eqs. (11)–(13) additional nonlinear terms appear in the relations for $\{\Delta, R_{ij}\}$ which are related to the full non-linear production terms for Maxwell molecules. The original derivation in Ref. 12 considered only linear production terms for Maxwell molecules; the omission of the non-linear production terms in the original equations is the reason why there were discrepancies in some super-Burnett coefficients.[15]

The system derived from the order of magnitude method to third order in Kn replaces the constitutive relations for the higher moments $R_{ij}$, $\Delta$, and $m_{ijk}$ by

$$\Delta = -\frac{\sigma_{kl}\sigma_{kl}}{\rho} + 6\frac{\sigma_{kl}\sigma_{kl}^{NSF}}{\rho} + \frac{56}{5}\frac{q_k q_k^{NSF}}{p} - 12\mu\theta\frac{\partial}{\partial x_k}\left(\frac{q_k}{p}\right), \tag{14}$$

$$R_{ij} = -\frac{4}{7}\frac{\sigma_{k\langle i}\sigma_{j\rangle k}}{\rho} + \frac{24}{7}\frac{\sigma_{k\langle i}\sigma_{j\rangle k}^{NSF}}{\rho} + \frac{64}{25}\frac{q_{\langle i}q_{j\rangle}^{NSF}}{p} - \frac{24}{5}\mu\theta\frac{\partial}{\partial x_{\langle i}}\left(\frac{q_{j\rangle}}{p}\right), \tag{15}$$

$$m_{ijk} = \frac{8}{15}\frac{\sigma_{\langle ij}q_{k\rangle}^{NSF}}{p} + \frac{4}{5}\frac{q_{\langle i}\sigma_{jk\rangle}^{NSF}}{p} - 2\mu\theta\frac{\partial}{\partial x_{\langle i}}\left(\frac{\partial\sigma_{jk\rangle}}{p}\right). \tag{16}$$

### C. The first modification to accommodate boundary conditions (2008)

Torrilhon and Struchtrup[16] proposed a system of boundary conditions for the R13 equations for simulating gas interaction with a solid wall at a given temperature and velocity, based on the microscopic boundary conditions for the Boltzmann equation, and the Grad distribution function that is used for closure of the bulk equations. The focus of their first study was on microflows, which allowed them to use a variant of the analytical expressions for $\Delta$, $R_{ij}$, and $m_{ijk}$. They simplified the original R13 equations (11)–(13); hence the non-linear terms from the production terms are missing. The first simplification is that they set the pressure gradient to zero, which for the problems considered in Ref. 16 leads to deviations of 4th order in Kn only but cannot be generalized to other microflow configurations. Thus, Eqs. (14)–(16) reduce to

$$\Delta = 6\frac{\sigma_{kl}\sigma_{kl}^{NSF}}{\rho} + \frac{56}{5}\frac{q_k q_k^{NSF}}{p} - 12\frac{\mu}{p}\frac{\partial q_k}{\partial x_k}, \tag{17}$$

$$R_{ij} = \frac{24}{7}\frac{\sigma_{k\langle i}\sigma_{j\rangle k}^{NSF}}{\rho} + \frac{64}{25}\frac{q_{\langle i}q_{j\rangle}^{NSF}}{p} - \frac{24}{5}\frac{\mu}{p}\frac{\partial q_{\langle i}}{\partial x_{j\rangle}}, \tag{18}$$

$$m_{ijk} = \frac{8}{15}\frac{\sigma_{\langle ij}q_{k\rangle}^{NSF}}{p} + \frac{4}{5}\frac{q_{\langle i}\sigma_{jk\rangle}^{NSF}}{p} - 2\frac{\mu}{p}\frac{\partial\sigma_{\langle ij}}{\partial x_{k\rangle}}. \tag{19}$$

The next simplification is the replacement of $\left\{\sigma_{ij}^{NSF}, q_i^{NSF}\right\}$ by $\left\{\sigma_{ij}, q_i\right\}$ in Eqs. (17)–(19), which does not change the order of accuracy of these equations, i.e., they still yield the correct super-Burnett equations. However, this change alters the mathematical properties of these equations such that linear and non-linear equations require the same number of boundary conditions. With this, the same set of boundary conditions can be used for linear and non-linear problems. The required number of boundary conditions matches the number of boundary conditions that arises naturally from the procedure outlined above.[16]

This nonlinear variant of the R13 equations can be expected to be rather problematic, due to the above-mentioned simplifications, in particular the assumption of constant pressure. It is obvious that this modification is problematic for studying nonlinear problems such as shock structures. Nevertheless, we decided to check the area of applicability of this variant and the variant with the replacement of $\left\{\sigma_{ij}^{NSF}, q_i^{NSF}\right\}$ by $\left\{\sigma_{ij}, q_i\right\}$.

The question of formulating proper boundary conditions for the R13 equations is under ongoing investigation.[27]

### D. Modified order of magnitude closure (2013)

The most recent variant of the R13 equations[17] is based on the variant of 2005 (14)–(16), only that $\left\{\sigma_{ij}^{NSF}, q_i^{NSF}\right\}$ is again replaced by $\left\{\sigma_{ij}, q_i\right\}$ in order to preserve the order of accuracy of the equations. With this substitution, linear and non-linear equations require the same number of boundary conditions. The difference to the equations in Sec. II C is that the pressure is not restricted; hence this variant has a wider range of applications. Notably, this variant was successfully applied for simulating slow steady transitional flows in a cavity.[17] The constitutive equations read

$$\Delta = 5\frac{\sigma_{kl}\sigma_{kl}}{\rho} + \frac{56}{5}\frac{q_k q_k}{p} - 12\mu\theta\frac{\partial}{\partial x_k}\left(\frac{q_k}{p}\right), \tag{20}$$

$$R_{ij} = \frac{20}{7}\frac{\sigma_{k\langle i}\sigma_{j\rangle k}}{\rho} + \frac{64}{25}\frac{q_{\langle i}q_{j\rangle}}{p} - \frac{24}{5}\mu\theta\frac{\partial}{\partial x_{\langle i}}\left(\frac{q_{j\rangle}}{p}\right), \tag{21}$$

$$m_{ijk} = \frac{4}{3}\frac{\sigma_{\langle ij}q_{k\rangle}}{p} - 2\mu\theta\frac{\partial}{\partial x_{\langle i}}\left(\frac{\sigma_{jk\rangle}}{p}\right). \tag{22}$$

## III. NUMERICAL RESULTS AND DISCUSSIONS

Previously, only the linear variant of the R13 system (10)[28,29] and the nonlinear variant (11)–(13) were used for supersonic flows in general, and for the problem of the shock wave structure in particular, whereas the fourth-order terms with respect to the Knudsen numbers were neglected.[25,26] Numerical results for the R13 system and DSMC computations are obtained in a wide range of Mach numbers ($1.0 < \mathrm{M} < 8.0$). In this section, we report results for all nonlinear variants of the R13 system discussed above. These results are compared with reference data computed by the DSMC method.

### A. Formulation of the problem

A one-dimensional plane shock wave problem is considered with flow from left to right, where the free-stream gas-dynamic variables $\rho_1$, $v_{x1}$, and $T_1$ (on the left) are the input parameters. To impose the boundary conditions on the subsonic right boundary, the corresponding values $\rho_2$, $v_{x2}$, and $T_2$ are calculated from the free-stream parameters $\rho_1$, $v_{x1}$, and $T_1$ with the use of conservation equations (Rankine-Hugoniot conditions)[1]

$$\rho v_x = const,\ \rho v_x^2 + p = const,\ \frac{v_x^2}{2} + h = const., \tag{23}$$

where $h$ is enthalpy; for a monatomic gas $h = \frac{5}{2}RT$, with $R = \frac{k}{m}$.

All results presented further are in the dimensionless form. The temperature and density are normalized in accordance to the formulas

$$\bar{T} = \frac{T - T_1}{T_2 - T_1},\ \bar{\rho} = \frac{\rho - \rho_1}{\rho_2 - \rho_1}. \tag{24}$$

With this, the macroparameters on the upstream and downstream boundaries have the values of 1 and 2, respectively.

### B. Numerical scheme

The numerical method used for solving the various variants of the R13 system in this work was described in detail in Refs. 26 and 29. A high-order Godunov scheme is used for computing the internal spatial cells. The viscosity coefficient is calculated by the power-law formula

$$\mu = \mu_0\left(\frac{T}{T_0}\right)^{\omega}, \tag{25}$$

where $0.5 \le \omega \le 1.0$. The values $\omega = 0.5$ and $\omega = 1.0$ correspond to the models of hard spheres and Maxwell molecules, respectively;[3] all computations presented in this paper were performed for Maxwell molecules.

The DSMC computations were performed by the SMILE++ software system[30,31] which is based on the majorant frequency scheme.[32] Molecular interaction is described by the Variable Hard Sphere (VHS) model,[20] which corresponds to the model of hard spheres for $\omega = 0.5$ and to the model of pseudo-Maxwell molecules for $\omega = 1.0$; in the latter case, molecular scattering is isotropic, in contrast to the model of Maxwell molecules. It has been demonstrated that these two models (Maxwell molecules and VHS with $\omega = 1.0$) predict identical profiles of gas dynamic parameters in shock waves for Mach numbers up to 10.[33,34] Furthermore, in the paper, all results for Maxwell molecules were obtained by the DSMC method with the VHS model for $\omega = 1.0$.

For the clarification of results' readability, see the table with the list of presented R13 variants and its corresponding notations in Table I.

TABLE I. R13 variants and its corresponding notations.

| Notations in the figures | Description | Numbers of the equations |
|---|---|---|
| R13 2003 full | Original variant | (11)–(13) |
| R13 2003 restricted | Original variant without 4th order corrections | (11)–(13) without underlined terms |
| R13 2005 | Order of magnitude closure modification | (14)–(16) |
| R13 2008 with NSF | Boundary condition modification | (17)–(19) |
| R13 2008 without NSF | Simplified boundary condition modification | (17)–(19) with $\left\{\sigma_{ij}^{NSF}, q_i^{NSF}\right\} = \left\{\sigma_{ij}, q_i\right\}$ |
| R13 2013 | Modified order of magnitude closure variant | (20)–(22) |

### C. Results for M = 2.0

For weak shock waves, at Mach number M = 2.0, results for shock structures were obtained for all R13 variants described above. The density and temperature profiles obtained by solving the R13 system are compared in Fig. 1 to the reference DSMC data. It is seen that all R13 versions work well in this regime. It should be noted that even the modification (17)–(19) with the replacement of $\left\{\sigma_{ij}^{NSF}, q_i^{NSF}\right\}$ by $\left\{\sigma_{ij}, q_i\right\}$, which was used in Ref. 16 for steady gas flows in microchannels, gives good agreement with the DSMC results for this Mach number (shown in Fig. 1(b), indicated as R13 2008 without NSF). Typically, it is easier to match lower moments, such as density and temperature, while higher moments deviate more from exact solutions. Nevertheless, comparing the profiles of stress tensor component $\sigma_{xx}$ and heat flux $q_x$ (Fig. 2) the picture is very similar, with good agreement between all R13 solutions and DSMC.

In summary, it is fair to state that all variants of the R13 equations provide sufficiently accurate results for shock structures at M = 2. It should be noted that weak shocks are relatively wide; hence the associated Knudsen number based on the mean free path and shock width is relatively small. Since all R13 variants agree in asymptotic expansions (specifically, Chapman-Enskog to 3rd order), agreement is expected for sufficiently small Knudsen numbers.

### D. Results for M = 4.0

The same comparison is performed in Figs. 3 and 4 for stronger shocks, with the Mach number M = 4.0. As the shock wave becomes stronger, nonlinear terms contribute more, and the predicted profiles become appreciably different. As could be expected, the worst result is provided by the roughest variant, which is the modification of the R13 system applied to subsonic flows in microchannels in Ref. 16. Replacement of $\left\{\sigma_{ij}^{NSF}, q_i^{NSF}\right\}$ by $\left\{\sigma_{ij}, q_i\right\}$, which is also used in the variant of 2013, yields significantly deteriorated results for the temperature, stress tensor component, and heat flux profiles.

While the subsonic part of the shock wave structure (trailing edge, on the right of the figures) can be considered acceptable, the results of last modifications of R13 (versions (17)–(22)) for the supersonic part (front edge) become extremely unphysical.

Concerning the earlier R13 variants, the original variant with allowance for the fourth-order terms with respect to the Knudsen number provides the best results. This is observed for all investigated macroparameters, including accurate prediction of the maxima of $\sigma_{xx}$ and $q_x$ in the shock. Nevertheless, visible differences to the DSMC data in the solution of this variant are observed in the beginning of supersonic part of the shock.

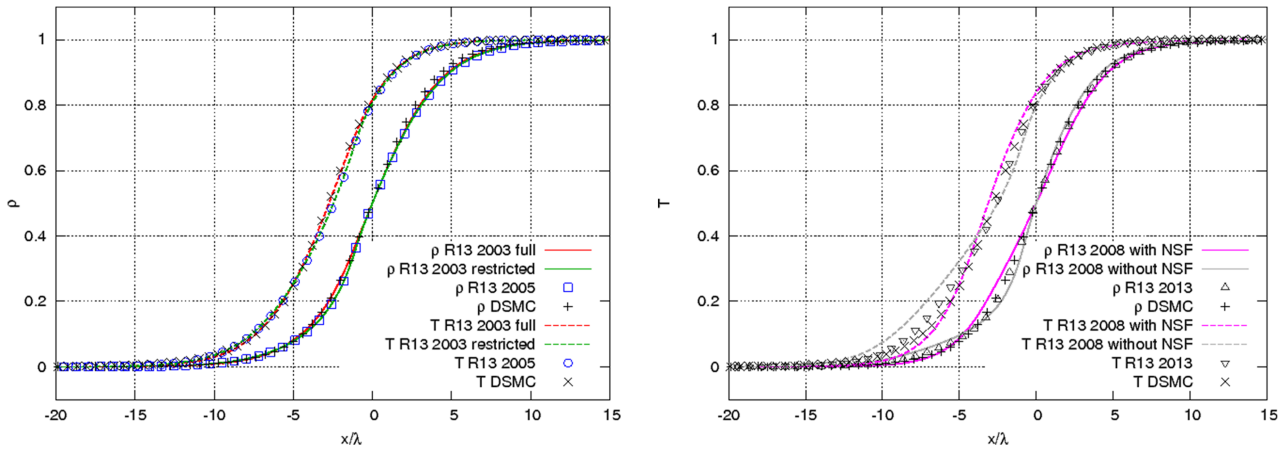


(a) (b)

FIG. 1. Comparison of R13 density and temperature profiles with DSMC data for M = 2.0. (a) Original variant (2003 full), the same variant without 4th order corrections (2003 restricted), and the order of magnitude closure modification (2005). (b) Boundary condition modification (2008 with NSF), the same with $\left\{\sigma_{ij}^{NSF}, q_i^{NSF}\right\} = \left\{\sigma_{ij}, q_i\right\}$ (2008 without NSF), and modified order of magnitude closure variant (2013).

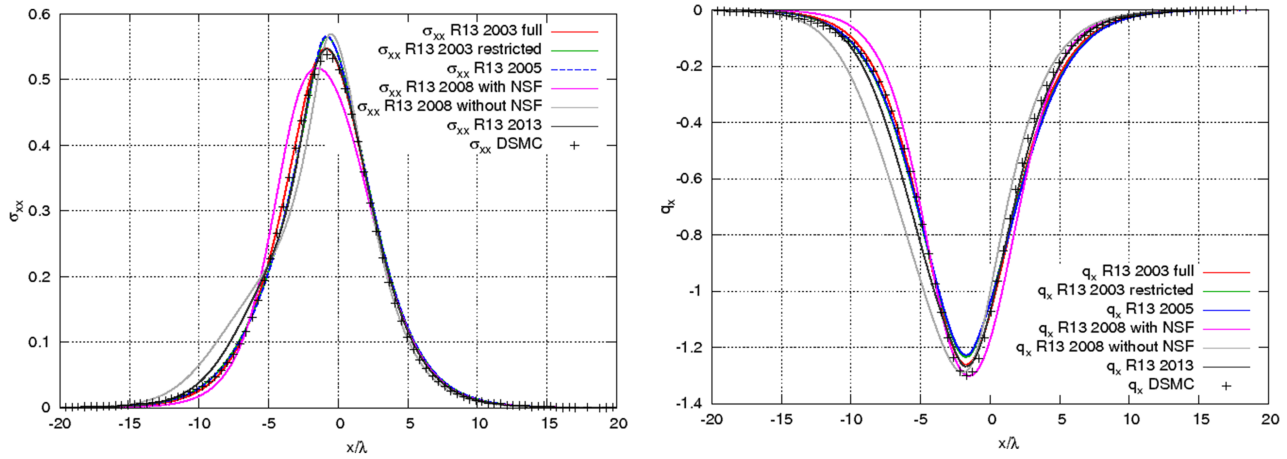


(a) (b)

FIG. 2. Comparison of R13 $\sigma_{xx}$ (a) and $q_x$ (b) profiles with DSMC data for M = 2.0. Original variant (2003 full), the same variant without 4th order corrections (2003 restricted), order of magnitude closure modification (2005), boundary condition modification (2008 with NSF), the same with $\left\{\sigma_{ij}^{NSF}, q_i^{NSF}\right\} = \left\{\sigma_{ij}, q_i\right\}$ (2008 without NSF), and modified order of magnitude closure variant (2013).

When we turn our attention to the results of the original version R13 (2003) and those modified in 2005 with the inclusion of $\left\{-\frac{\sigma_{ij}\sigma_{ij}}{\rho}, -\frac{4}{7}\frac{\sigma_{k\langle j}\sigma_{j\rangle k}}{\rho}\right\}$, it can be seen that the inclusion of these additional nonlinear terms in Eqs. (14)–(16) does not exert any significant influence on the curves. It should be noted that for this Mach number a point emerges around $x/\lambda = -5$ in the curves which exhibit a kink-like drastic change in steepness.

### E. Results for M = 8.0

The difference between the kinetic approach data and R13 moment equations solutions grows significantly when going to the hypersonic regime (M = 8.0, Figs. 5 and 6). The simplified versions of 2008 and 2013 with the replacement $\left\{\sigma_{ij}^{NSF}, q_i^{NSF}\right\} = \left\{\sigma_{ij}, q_i\right\}$, which were already problematic for M = 4.0, yield even worse results for M = 8.0. This is why the results for these R13 modifications are not shown.

The results of the earlier modifications of 2003 without $\mathrm{Kn}^4$ corrections and 2005 can be hardly distinguished (Figs. 5 and 6), similar to the situation for M = 4.0. The difference between the results of R13 and DSMC becomes more obvious for all curves, density and temperature profiles (Fig. 5), and the profiles of $\sigma_{xx}$ and heat flux (Fig. 6). The kink-like change in steepness in the temperature and density curves at the center of the shock wave (at about $x/\lambda = -2$) becomes even more noticeable. This special point will be considered in more detail below. Nevertheless, while the details differ, the moment approach ensures reasonable qualitative agreement with DSMC results even for this Mach number.

At the same time, the original version of 2003, which includes the terms of $Kn^4$ order, still allows to get the best result. These amendments, as well as in the case of M = 4.0,

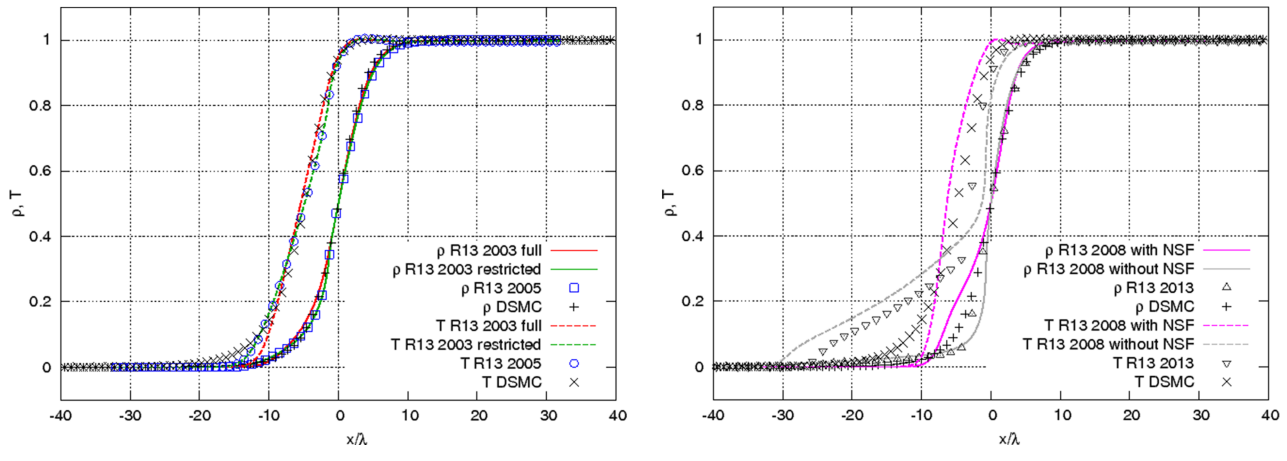


(a) (b)

FIG. 3. Comparison of R13 density and temperature profiles with DSMC data for M = 4.0. (a): Original variant (2003 full), the same variant without 4th order corrections (2003 restricted), and order of magnitude closure modification (2005). (b): Boundary condition modification (2008 with NSF), the same with $\left\{\sigma_{ij}^{NSF}, q_i^{NSF}\right\} = \left\{\sigma_{ij}, q_i\right\}$ (2008 without NSF), and modified order of magnitude closure variant (2013).

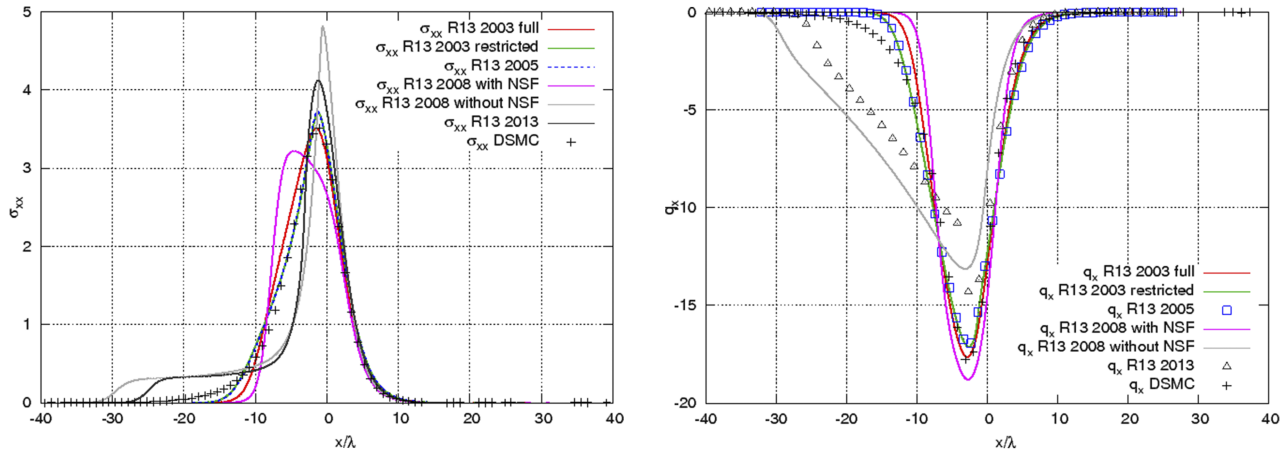


(a) (b)

FIG. 4. Comparison of R13 $\sigma_{xx}$ (a) and $q_x$ (b) profiles with DSMC data for M = 4.0. Original variant (2003 full), the same variant without 4th order corrections (2003 restricted), the order of magnitude closure modification (2005), boundary condition modification (2008 with NSF), the same with $\left\{\sigma_{ij}^{NSF}, q_i^{NSF}\right\} = \left\{\sigma_{ij}, q_i\right\}$ (2008 without NSF), and the modified order of magnitude closure variant (2013).

do not render a strong influence on the profiles of the macroparameters in the subsonic part of the shockwave structure, but they significantly affect the supersonic area. The profile of density of this variant converges similar with the DSMC data (Fig. 5(a)), and we see improvement in maxima component of the stress tensor $\sigma_{xx}$ and the heat flux $q_x$ (Fig. 6). Most importantly, this variant of the R13 equations allows removing an unnatural kink in the center of the shock wave from the solution (at the point of transition from the supersonic regime to the subsonic one, see Sec. III F).

We have decided to pay attention to the best variants (original 2003 variant, the same one without 4th Kn order contribution, 2008 boundary condition modification without the simplification $\left\{\sigma_{ij}^{NSF}, q_i^{NSF}\right\} = \left\{\sigma_{ij}, q_i\right\}$). The results are presented in Figs. 7–10. The relative error for each macroparameter ($y = \{\rho, T, \sigma_{xx}, q_x\}$) was counted as

$$\delta y = \max\left(\left|\frac{y_{R13} - y_{DSMC}}{y_{DSMC(\max)}}\right|\right) \cdot 100\%. \qquad (26)$$

According to these figures, 2003 variant without 4th order Kn contributions (or 2005 variant) shows formally a little bit better results for $\sigma_{xx}$ and $q_x$ for Mach M = 4.0 and for M = 8.0 than the original 2003 modification. At the same time, this bigger difference is observed in a small high velocity (supersonic for M = 4.0 or even hypersonic for M = 8.0) area of a shock wave structure, while the rest part of the structure is much better for original 2003 equations with 4th order *Kn* contribution.

### F. Kinks in the R13 solution

As mentioned before, shock solutions for Grad's 13 moment system exhibit sub-shocks, i.e., discontinuities in the variables, which appear for Mach numbers above 1.65.[13,35] While the variables of the R13 equations remain continuous, the 2003 and 2005 variants of the R13 equations (Eqs. (11)–(16)) exhibit kinks in the curves, which correspond to discontinuities in the derivatives of the variables, not

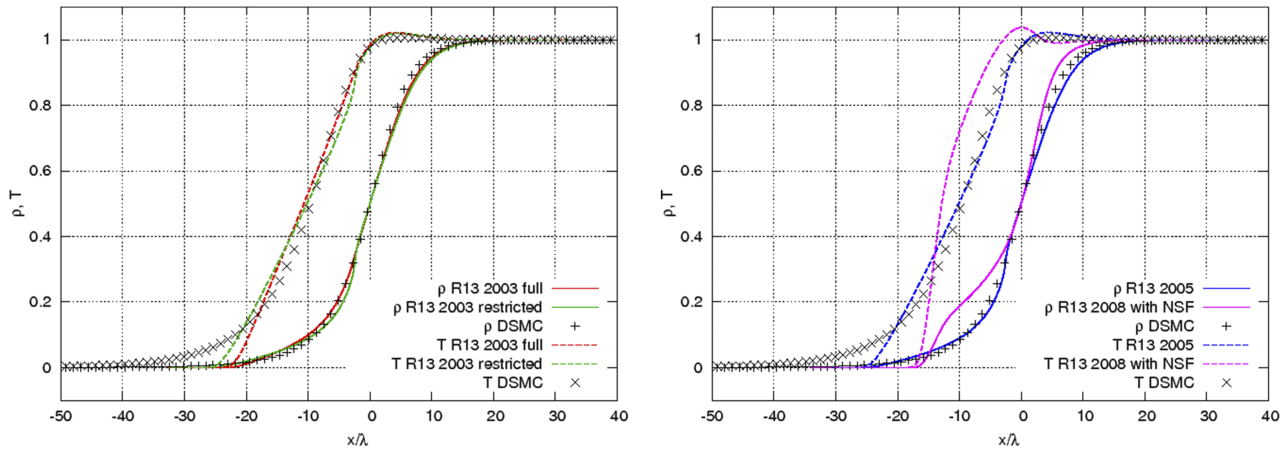


(a) (b)

FIG. 5. Comparison of R13 density and temperature profiles with DSMC data for M = 8.0. (a) Original variant (2003 full), the same variant without 4th order corrections (2003 restricted). (b) Boundary condition modification (2008 with NSF) and the order of magnitude closure modification (2005).

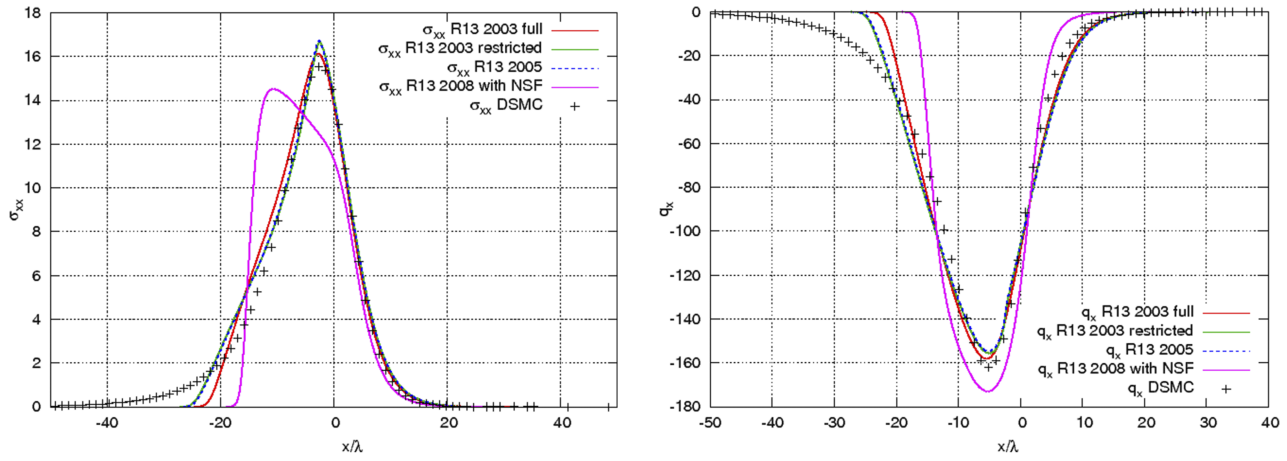


(a) (b)

FIG. 6. Comparison of R13 $\sigma_{xx}$ (a) and $q_x$ (b) profiles with DSMC data for M = 8.0. Original variant (2003 full), the same variant without 4th order corrections (2003 restricted), the order of magnitude closure modification (2005), boundary condition modification (2008 with NSF).

the variables themselves. The differences between both variants are rather small.

Figure 11 shows the curves for the variables (density, temperature, stress, heat flux) and the Mach number at M = 4 and M = 8. It is observed that the kinks in all curves appear at the transition point from the subsonic to supersonic regime, where the local Mach number is M = 1. A regularizing parameter $\varepsilon$ can be used to convert the R13 equations (for $\varepsilon = 1$) to the Grad 13 equations (for $\varepsilon = 0$);[3,15] hence the equations are strongly related. However, the locations of the sub-shocks in the Grad 13 equations are different from the location of the kinks for R13; hence it can be argued that both

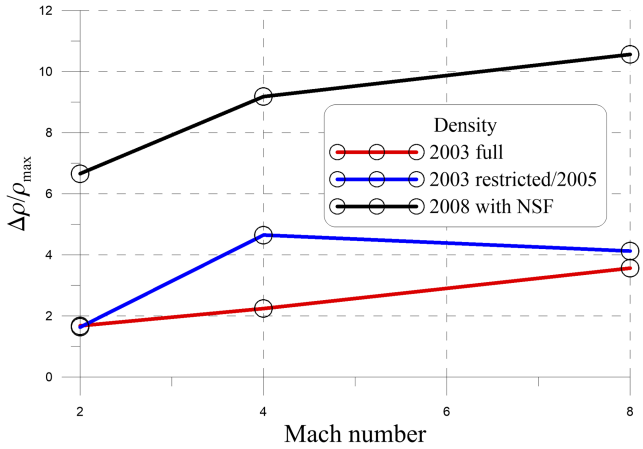


FIG. 7. Relative error for density.

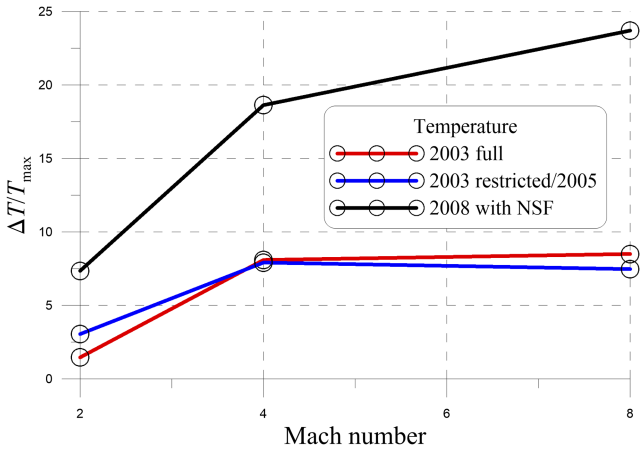


FIG. 8. Relative error for temperature.

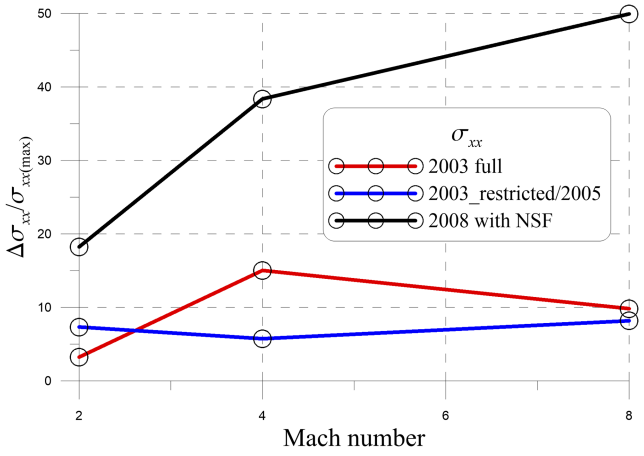


FIG. 9. Relative error for $\sigma_{xx}$.

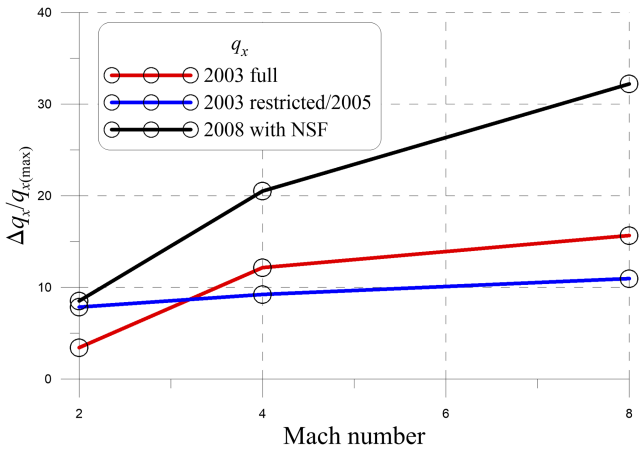


FIG. 10. Relative error for $q_x$.

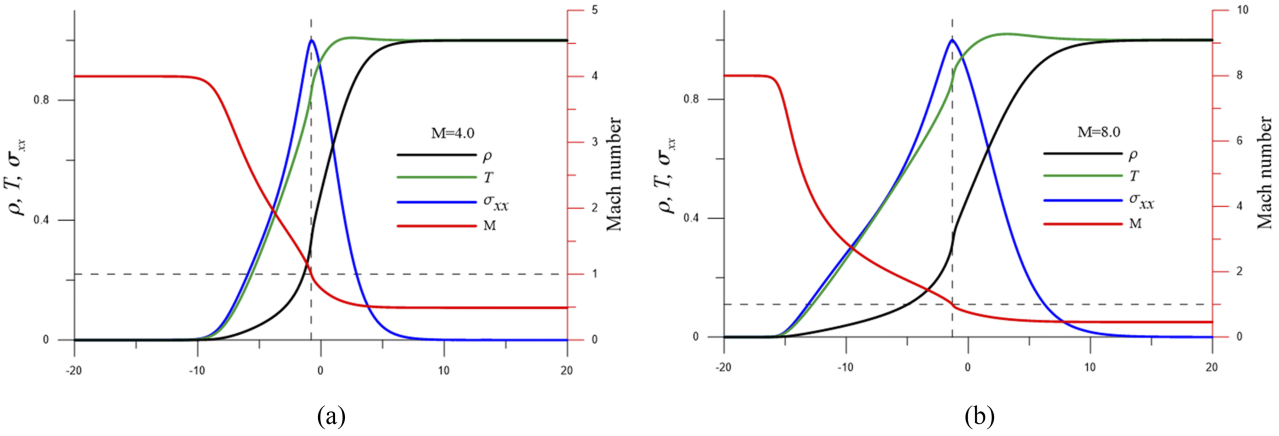


FIG. 11. Macroparameters' profiles inside the shock for M = 4.0 (a) and M = 8.0 (b), obtained with original R13 (2003/2005).

are independent effects due to the structure of the respective equations.

At the same time, it is interesting that there is no special point in the case of including of higher order Knudsen number terms ($Kn^4$ order) in these relations.

### G. Local Knudsen number as a function of the Mach number

The Knudsen number, which is the ratio of the mean free path to the reference length scale of the considered problem, is the basic measure of gas rarefaction. It is also convenient to use this similarity parameter for estimating the degree of flow non-equilibrium. The difficulty in applying the classical definition of the Knudsen number in the problem of the shock wave structure is the absence of an obvious reference length scale. An alternative for the classical definition is the use of the so-called local Knudsen number

$$Kn_Q = \frac{\lambda}{Q}\left|\frac{dQ}{dl}\right|, \tag{27}$$

where $\lambda$ is the mean free path, $Q$ stands for any macroparameter of interest (density, temperature, etc.), and $l$ is the spatial direction with the greatest growth of this parameter.

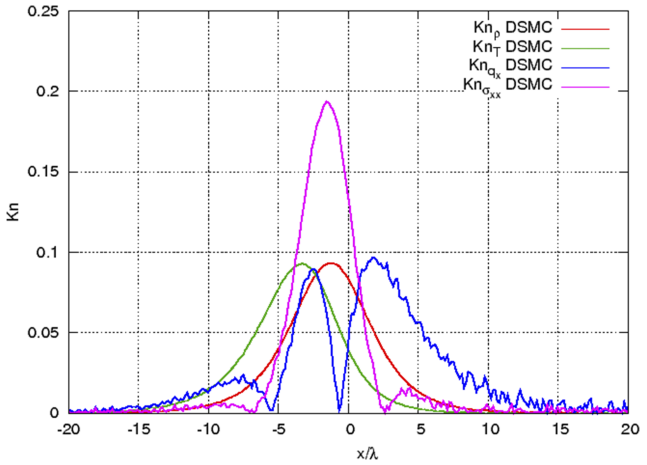


FIG. 12. Distribution of the local Knudsen number $Kn_\rho$, $Kn_T$, $Kn_{\sigma_{xx}}$, and $Kn_{q_x}$ for the Mach number M = 2.0. The results are based on DSMC computations.

The shock thickness is typically defined based on the maximum density gradient in the shock;[2,3] the corresponding Knudsen number for the shock is the maximum of the Knudsen number $Kn_\rho$ in the shock wave.[3,36] $Kn_\rho$ changes with the Mach number, but its maximum value does not exceed 0.2 for the Maxwell gas and, for instance, is smaller than 0.3 for

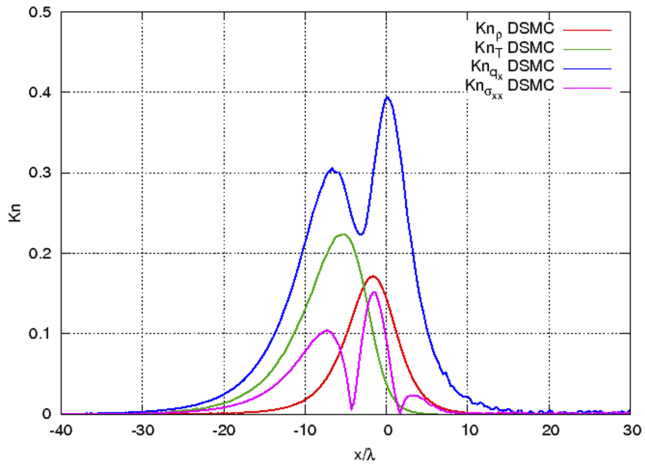


FIG. 13. Distribution of local Knudsen numbers $Kn_\rho$, $Kn_T$, $Kn_{\sigma_{xx}}$, and $Kn_{q_x}$ for the Mach number M = 4.0. The results are based on DSMC computations.

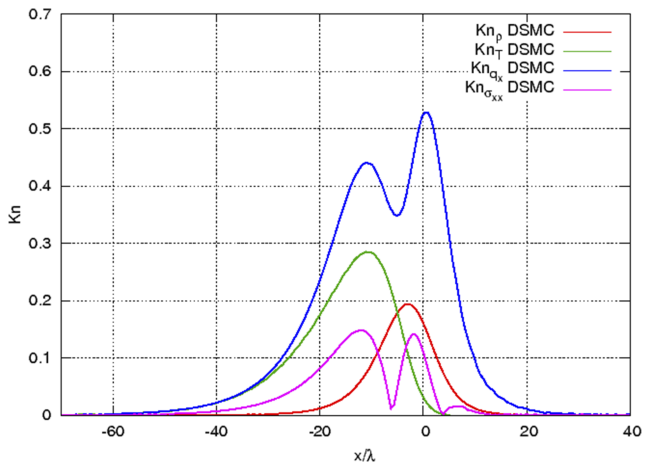


FIG. 14. Distribution of local Knudsen numbers $Kn_\rho$, $Kn_T$, $Kn_{\sigma_{xx}}$, and $Kn_{q_x}$ for the Mach number M = 8.0. The results are based on DSMC computations.

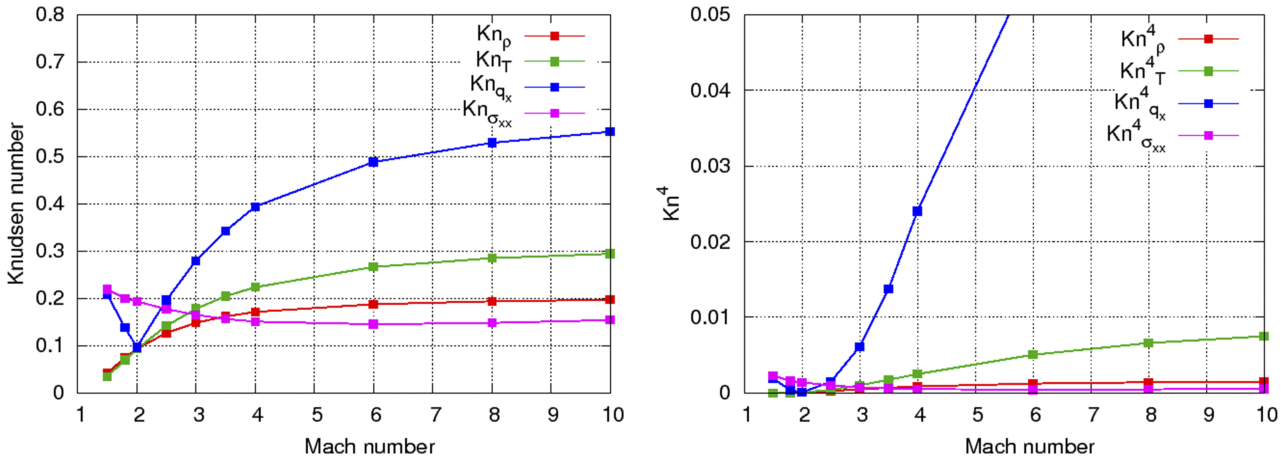


FIG. 15. Distribution of the maximum local Knudsen numbers $Kn_\rho$, $Kn_T$, $Kn_{\sigma_{xx}}$, and $Kn_{q_x}$ as functions of the Mach number (a), and distribution of the maximum values of $Kn^4_\rho$, $Kn^4_T$, $Kn^4_{\sigma_{xx}}$, and $Kn^4_{q_x}$ (b). The results are based on DSMC computations.

argon.[3,36] Some publications consider the local Knudsen number based on the temperature profile, $Kn_T$, where the value of $Kn_T$ is significantly different from $Kn_\rho$.[37]

Considering the local Knudsen number as an indicator of local flow non-equilibrium, it is interesting to evaluate and compare its values not only for temperature and density but also for non-equilibrium quantities such as the components of stress and heat flux. In Ref. 38, it was proposed to calculate the local Knudsen number for stress and heat flux, based on their deviation from the Navier-Stokes-Fourier relations, as

$$Kn_{\sigma_{xx}} = \frac{\left|\sigma_{xx} - \sigma_{xx}^{NSF}\right|}{\max\left(\sigma_{xx}^{NSF}\right)}, \quad \sigma_{xx}^{NSF} = -\frac{4}{3}\mu\frac{\partial v_x}{\partial x},$$
$$Kn_{q_x} = \frac{\left|q_x - q_x^{NSF}\right|}{\max\left(\left|q_x^{NSF}\right|\right)}, \quad q_x^{NSF} = -\frac{15}{4}\mu\frac{\partial \theta}{\partial x}. \tag{28}$$

Figures 12–14 show the distributions of the local Knudsen numbers $Kn_\rho$, $Kn_T$, $Kn_{\sigma_{xx}}$, and $Kn_{q_x}$ calculated from the DSMC simulations of shock wave structures with Mach numbers M = 2.0, 4.0, and 8.0. The values of $Kn_\rho$ and $Kn_T$ are calculated from the density and temperature profiles using (27), and $Kn_{\sigma_{xx}}$ and $Kn_{q_x}$ are calculated according to the profiles of stress tensor component $\sigma_{xx}$ and longitudinal heat flux component using (28).

Based on these distributions, it is evident that the value of the local Knudsen number depends strongly on the choice of the macroparameter used in its definition. To describe the rarefaction and non-equilibrium of a shock wave by a single Knudsen number, the most conservative approach would be to choose the largest value of any local Knudsen number. Figure 15(a) shows the distribution of the maximum values of $Kn_\rho$, $Kn_T$, $Kn_{\sigma_{xx}}$, and $Kn_{q_x}$ as functions of the shock wave Mach number, again calculated from DSMC data. As it is seen from Fig. 15(a), the values of $Kn_{\sigma_{xx}}$ and $Kn_\rho$ do not experience significant changes with shock wave enhancement; in the examined range of Mach numbers both remain below 0.2. The behavior of $Kn_{q_x}$ is the most interesting, with a minimum at M = 2.0 and a subsequent monotonic increase for Mach numbers M > 2.0. For larger Mach numbers, the values of $Kn_{q_x}$ are significantly larger than those of the other local Knudsen numbers.

The R13 moment equations are third-order equations with respect to the Knudsen number. Thus, if this moment approach is used, for the modeled flow the value of $Kn^4$ should be sufficiently small, with values below a threshold of about 0.05 (corresponding to Kn = 0.47). Figure 15(b) shows the distribution of the maximums of $Kn^4_\rho$, $Kn^4_T$, $Kn^4_{\sigma_{xx}}$, and $Kn^4_{q_x}$. The distribution of $Kn^4_{q_x}$ is the most interesting since it gives the largest value among the local Knudsen numbers. The value of $\mathrm{Kn}^4 = 0.05$ for the other investigated local Knudsen numbers is significantly smaller. Based on these considerations, with the threshold chosen as $\mathrm{Kn}^4 = 0.05$, the formal upper boundary of applicability of the R13 system for supersonic flows is for Mach numbers $M \approx 5.5$ (or Ma = 3.3 for the threshold 0.01). As a whole, this conclusion is confirmed by comparisons of the macroparameter profiles given above. On the other hand, the full nonlinear variant of the R13 system offers a possibility of obtaining good qualitative agreement with DSMC data for stronger shock waves as well.

## IV. CONCLUSIONS

We summarize our findings on the applicability of the R13 variants to shock waves. First, all nonlinear variants of the R13 system considered in this paper are applicable for simulations of weak shock waves since the various modifications exert only a minor effect on results for M = 2.0. However, the pattern becomes significantly different toward the range of hypersonic velocities. If the influence of the fourth-order terms with respect to the Knudsen number is not considered, the original variant of the R13 system (2003) is preferable for supersonic flow simulations. The nonlinear terms $\left\{-\frac{\sigma_{ij}\sigma_{ij}}{\rho}, -\frac{4}{7}\frac{\sigma_{k\langle j}\sigma_{j\rangle k}}{\rho}\right\}$ introduced in 2005,[3] which allow obtaining correct coefficients for super-Burnett equations, do not exert noticeable effects in the entire range of Mach numbers considered.

The modifications proposed after 2005 were driven by the desire to use the same boundary conditions for linear and non-linear equations. Since these equations yield unsatisfactory results for strong shock waves, they should not be used for strongly supersonic flows. This conclusion points to the necessity to revise the formulation of the boundary conditions of the R13 system on solid walls, in the case of strong supersonic flows. Due to gas-wall interaction, the gas close to the boundary will be relatively slow (relative to the wall), and a hybrid method seems possible, where the modified equations are used in the close vicinity of the wall, and the original equations away from the wall.

The fourth-order corrections with respect to the Knudsen numbers included into the high-order relations in Eqs. (11)–(13) ensure a significant improvement of results for all Mach numbers considered. The corrections help to improve the solution especially in the supersonic part and remove the macroparameter kinks in the shock wave center for higher Mach numbers.

In this study, we obtained the Knudsen number distributions based on $\sigma_{xx}$ and $q_x$ as functions of the Mach number. These data allow us to argue that there is a formal upper boundary of applicability for the mathematical model of the R13 equations. This formal boundary is confirmed by comparisons of the shock wave macroparameter profiles calculated with the use of the original R13 system with DSMC data for chosen Mach numbers. On the other hand, even beyond this upper boundary at $M \approx 5.5$, the original variant of the R13 system can still be used for the qualitative simulation of supersonic flows if there is no need for obtaining a detailed description of the internal structure of the shock wave.

## ACKNOWLEDGMENTS

This work was supported by Russian Foundation for Basic Research (Project Nos. 16-31-60034 and 16-38-50246) and the Natural Sciences and Engineering Research Council (NSERC). The work carried out at ITAM was supported by the Russian Science Foundation (Grant No. 15-19-30016).

[1]L. I. Sedov, *Mechanics of Continuous Media* (World Scientific, 1997).
[2]S. Chapman and T. G. Cowling, *The Mathematical Theory of Non-Uniform Gases: An Account of the Kinetic Theory of Viscosity, Thermal Conduction and Diffusion in Gases* (Cambridge Mathematical Library, 1991).
[3]H. Struchtrup, *Macroscopic Transport Equations for Rarefied Gas Flows* (Springer, 2005).
[4]M. N. Kogan, *Rarefied Gas Dynamics* (Plenum, New York, 1969).
[5]H. Grad, "On the kinetic theory of rarefied gases," Commun. Pure Appl. Math. **2**, 331–407 (1949).
[6]D. Burnett, "The distribution of molecular velocities and the mean motion in a non-uniform gas," Proc. London Math. Soc. **40**, 382–435 (1936).
[7]M. Sh. Shavaliyev, "Super-burnett corrections to the stress tensor and the heat flux in a gas of Maxwellian molecules," J. Appl. Math. Mech. **57**, 573–576 (1993).
[8]A. V. Bobylev, "The Chapman-Enskog and Grad methods for solving the Boltzmann equation," Sov. Phys. Dokl. **27**, 29–31 (1982).
[9]H. Struchtrup, "Failures of the Burnett and super-Burnett equations in steady state processes," Continuum Mech. Thermodyn. **17**, 43–50 (2005).
[10]A. V. Bobylev, "Instabilities in the Chapman-Enskog expansion and hyperbolic Burnett equations," J. Stat. Phys. **124**, 371–399 (2006).
[11]L. H. Söderholm, "Hybrid Burnett equations: A new method of stabilizing," Transp. Theory Stat. Phys. **36**, 495–512 (2007).
[12]H. Struchtrup and M. Torrilhon, "Regularization of Grad's 13-moment equations: Derivation and linear analysis," Phys. Fluids **15**, 2668–2680 (2003).
[13]I. Müller and T. Ruggeri, *Rational Extended Thermodynamics*, Springer Tracts in Natural Philosophy Vol. 37 (Springer, New York, 1998).
[14]M. Torrilhon, "Characteristic waves and dissipation in the 13-moment-case," Continuum Mech. Thermodyn. **12**, 289–301 (2000).
[15]M. Torrilhon and H. Struchtrup, "Regularized 13-moment equations: Shock structure calculations and comparison to Burnett models," J. Fluid Mech. **513**, 171–198 (2004).
[16]H. Struchtrup and M. Torrilhon, "Boundary conditions for regularized 13-moment equations for microchannel flows," J. Comput. Phys. **227**, 1982–2011 (2008).
[17]A. S. Rana, M. Torrilhon, and H. Struchtrup, "A robust numerical method for the R13 equations of rarefied gas dynamics: Application to lid driven cavity," J. Comput. Phys. **236**, 169–186 (2013).
[18]H. Struchtrup and P. Taheri, "Macroscopic transport models for rarefied gas flows: A brief review," IMA J. Appl. Math. **76**(5), 672–697 (2011).
[19]M. Torrilhon, "Modeling nonequilibrium gas flow based on moment equations," Annu. Rev. Fluid Mech. **48**, 429–458 (2016).
[20]G. A. Bird, *Molecular Gas Dynamics and the Direct Simulation of Gas Flows* (Oxford University Press, Oxford, 1994).
[21]E. A. Malkov, Ye. A. Bondar, A. A. Kokhanchik, S. O. Poleshkin, and M. S. Ivanov, "High-accuracy deterministic solution of the Boltzmann equation for the shock wave structure," Shock Waves **25**, 387–397 (2015).
[22]M. Yu. Timokhin, H. Struchtrup, A. A. Kokhanchik, and Ye. A. Bondar, "The analysis of different variants of R13 equations applied to the shock-wave structure," AIP Conf. Proc. **1786**, 140006 (2016).
[23]X. J. Gu and D. R. Emerson, "A high-order moment approach for capturing non-equilibrium phenomena in the transition regime," J. Fluid Mech. **636**, 177–216 (2009).
[24]M. Torrilhon, "Two-dimensional bulk microflow simulations based on regularized Grad's 13-moment equations," Multiscale Model. Simul. **5**(3), 695–728 (2006).
[25]I. E. Ivanov, I. A. Kryukov, M. Yu. Timokhin, Ye. A. Bondar, A. A. Kokhanchik, and M. S. Ivanov, "Study of shock wave structure by regularized Grad's set of equations," AIP Conf. Proc. **1501**, 215–222 (2012).
[26]M. Y. Timokhin, Ye. A. Bondar, A. A. Kokhanchik, M. S. Ivanov, I. E. Ivanov, and I. A. Kryukov, "Study of shock wave structure by regularized Grad's set of equations," Phys. Fluids **27**, 037101 (2015).
[27]A. S. Rana and H. Struchtrup, "Thermodynamically admissible boundary conditions for the regularized 13 moment equations," Phys. Fluids **28**, 027105 (2016).
[28]I. A. Znamenskaya, I. E. Ivanov, I. A. Kryukov, I. V. Mursenkova, and M. Yu. Timokhin, "Shock-wave structure formation by nanosecond discharge in helium," Tech. Phys. Lett. **40**, 533–536 (2014).
[29]I. E. Ivanov, I. A. Kryukov, and M.Yu. Timokhin, "Application of moment equations to the mathematical simulation of gas microflows," Comput. Math. Math. Phys. **53**, 1534–1550 (2013).
[30]A. V. Kashkovsky, Ye. A. Bondar, G. A. Zhukova, M. S. Ivanov and S. F. Gimelshein, "Object-oriented software design of real gas effects for the DSMC method," AIP Conf. Proc. **762**, 583–588 (2005).
[31]M. S. Ivanov, A. V. Kashkovsky, P. V. Vashchenkov, and Ye. A. Bondar, "Parallel object-oriented software system for DSMC modeling of high-altitude aerothermodynamic problems," AIP Conf. Proc. **1333**, 211–218 (2011).
[32]M. S. Ivanov and S. V. Rogasinsky, "Analysis of the numerical techniques of the direct simulation Monte Carlo method in the rarefied gas dynamics," Sov. J. Numer. Anal. Math. Modell. **3**, 453–465 (1988).
[33]G. A. Bird, "Definition of mean free path in real gases," Phys. Fluids **26**, 3222–3223 (1983).
[34]K. Koura and H. Matsumoto, "Variable soft sphere molecular model for inverse power law or Lennard-Jones potential," Phys. Fluids A **3**, 2459–2465 (1991).
[35]L. H. Holway, "Existence of kinetic theory solutions to the shock structure problem," Phys. Fluids **7**(6), 911–913 (1964).
[36]H. Alsmeyer, "Density profiles in argon and nitrogen shock waves measured by the absorption of an electron beam," J. Fluid Mech. **74**, 497–513 (1976).
[37]A. I. Erofeev and O. G. Friedlander, "Macroscopic models for nonequilibrium flows of monatomic gas and normal solutions," in *Proceedings of 25th International Symposium on RGD* (2007), pp. 117–124.
[38]D. A. Lockerby, J. M. Reese, and H. Struchtrup, "Switching criteria for hybrid rarefied gas flow solvers," Proc. R. Soc. A **465**, 1581–1598 (2009).